

Structural model updating of the Gageocho Ocean Research Station using mass reallocation method

Byungmo Kim¹⁾ and *Jin-Hak Yi²⁾

¹⁾ *Department of Convergence Study on the Ocean Science and Technology, Ocean Science and Technology School, Korea Maritime and Ocean University, Busan, South Korea*

²⁾ *Coastal Development and Ocean Energy Research Center, Korea Institute of Ocean Science and Technology, Busan, South Korea*

¹⁾ *airboy1004@kmou.ac.kr*

²⁾ *yjih@kiost.ac.kr*

ABSTRACT

To study oceanic and meteorological problems related to climate change, Korea has been operating several ocean research stations (ORSs). In 2011, the Gageocho ORS was attacked by Typhoon Muifa, and its structural members and several observation devices were severely damaged. After this event, the Gageocho ORS was rehabilitated with 5 m height to account for 100-yr extreme wave height, and the vibration measurement system was equipped to monitor the structural vibrational characteristics including natural frequencies and modal damping ratios. In this study, a mass reallocation method is presented for structural model updating of the Gageocho ORS based on the experimentally identified natural frequencies. A preliminary finite element (FE) model was constructed based on design drawings, and several of the candidate baseline FE models were manually built, taking into account the different structural conditions such as corroded thickness. Among these candidate baseline FE models, the most reasonable baseline FE model was selected by comparing the differences between the identified and calculated natural frequencies; the most suitable baseline FE model was updated based on the identified modal properties, and by using the pattern search method, which is one of direct search optimization methods. The mass reallocation method is newly proposed as a means to determine the equivalent mass quantities along the height and in a floor. It was found that the natural frequencies calculated based on the updated FE model was very close to the identified natural frequencies. In conclusion, it is expected that these results, which were obtained by updating a baseline FE model, can be useful for establishing the reference database for jacket-type offshore structures, and assessing the structural integrity of the Gageocho ORS.

¹⁾ Graduate Student

²⁾ Principal Research Scientist, Professor

1. INTRODUCTION

Ocean research stations (ORSs) play important roles as comprehensive oceanography laboratories that support diverse research ranging from long-term observations of marine physics, climates, environments, and marine biology, to typhoon and particulate matter tracking. There are three ORSs in operation in Korea, including the leodo, Gageocho, and Socheongcho ORSs that were respectively established in 2003, 2009, and 2014. They are located in the Yellow Sea between China and Korea (see Figure 1), because a wide variety of ocean and meteorological phenomena occur in these waters, such as typhoons and the transportation of particulate matter. The structural integrity of the ORS structures must be maintained to ensure that they remain stable during their design lifetime. However, in 2011, Typhoon Muifa critically damaged the Gageocho ORS; consequently, numerous components, such as data transmission cables and a diesel generator, were broken. A long time and extensive effort were required to rehabilitate them and enhance the overall structural integrity such that the ORS could resume normal operation. Figure 2(a) presents the Gageocho ORS before and after the damage in 2011 (Shim et al. 2015, Kim et al. 2017). The most significant structural modification was the heightening of the superstructure (i.e., up to 5 m), which was purposed to increase the clearance of the platform and thus prevent excessive uplifting owing to the force of abnormally high waves. For this purpose, four steel tubular members were newly fabricated and inserted between the superstructure and substructure of the Gageocho ORS. The diameter and thickness of the new members were larger than those of the existing members to ensure that the structural strength would be higher. To prevent such an accident from recurring after the reconstruction, a structural vibration monitoring system was implemented by installing sensors onto the Gageocho ORS for structural health monitoring (SHM); this was as one of measurement-based preventative maintenance ways.



Fig. 1 Locations of operational ORSs in South Korea

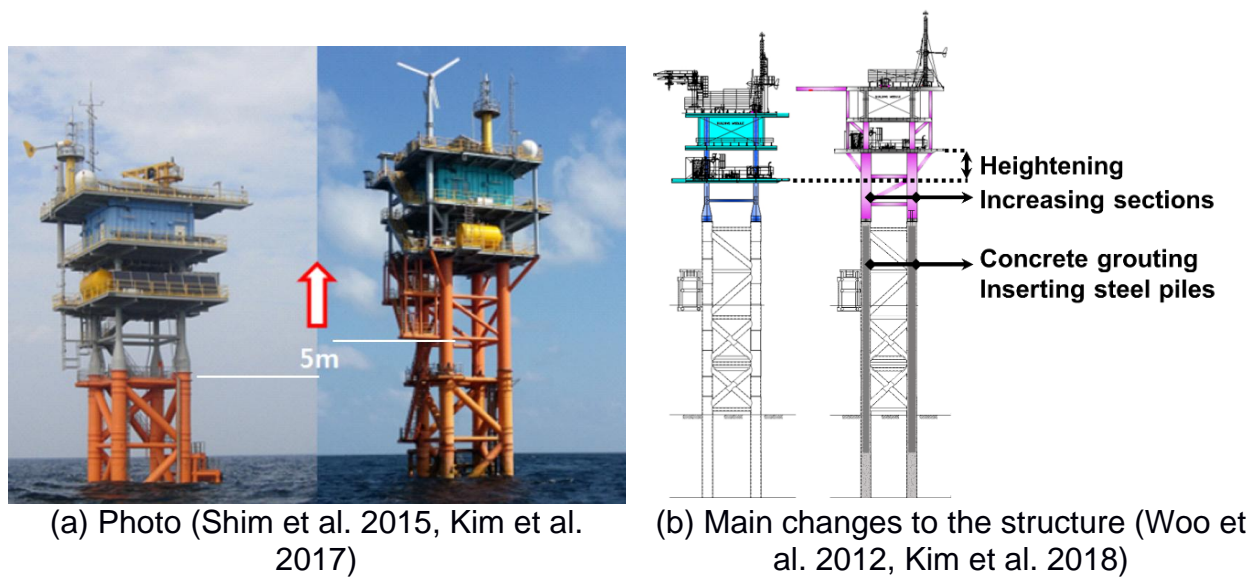


Fig. 2 Gageocho ORS before and after recovery::

There are two approaches for SHM (Cremona and Santos 2016). The first approach is forward-type, and the second approach is inverse-type. The former entails only using measured data for the evaluation of structural safety, whereas the latter entails utilizing a simulation model (hereafter referred to as the baseline model), such as a finite element (FE) model, in combination with sensing data; this approach is more common than the forward method. To further explain, the structural characteristics derived from measurements are compared to those derived from the baseline model; then, the cause of the differences between them are analyzed to assess the damage and current structural state. These are the processes of the general inverse SHM. Therefore, the most essential prerequisite for precise SHM is the establishment of an accurate baseline model, which is hereafter referred to as a model updating. Thus, the updating process shall be conducted in consideration of the structural characteristics that will be monitored in the next SHM cycle. Various features that reflect the structural states, such as static displacement, response to impact, or dynamic response, can be applied to SHM. Among these structural states, it is most common to utilize the vibrational characteristics, i.e., the natural frequencies and mode shapes, to monitor structural integrity (Fritzen et al. 2017). This is because they can be continuously analyzed based on measured dynamic responses without the information on excitation force which are very difficult or impossible to measure. In the case of the Gageocho ORS, the dynamic properties were also investigated by using the measured responses to analyze the structural system (Kim et al. 2017). Therefore, in this study, a baseline model of the Gageocho ORS that accurately simulates the natural frequencies that were measured during previous studies was developed as the first step of SHM to facilitate maintenance of the Gageocho ORS.

2. APPROACH TO MODEL UPDATE

2.1 Comparison of Measured Data and Preliminary Simulation Model Results

As with all other offshore structures, the preliminary numerical modeling and safety check for the Gageocho ORS were performed before the retrofit construction (Woo et al. 2012). In this study, the original model that was constructed by using a commercial offshore analysis program (SACS, Engineering Dynamics, Inc., 1995) was transformed into an FE model by using a commercial FE analysis program (ANSYS Mechanical APDL, ANSYS, Inc., 2017). Generally, there is a certain level of uncertainty and modeling error in the structural analysis model; thus, the results of analysis of the model simulation tend to disagree with the measured responses for the target structure. In the case of the Gageocho ORS, the calculated natural frequencies for the lowest five modes obtained from the preliminary FE model were much larger than the identified natural frequencies obtained via the measured responses, as shown in Table 1. Hence, it is vital to accurately update the FE model for successful SHM. Note that the 1st and 2nd modes correspond to the 1st bending mode in two perpendicular directions, the 3rd mode is the 1st torsional mode of the Gageocho ORS, and the 4th and 5th modes correspond to the 2nd bending mode in the perpendicular directions. It should also be noted that the difference between two natural frequencies corresponding to the same mode is due to the eccentricity of mass distribution.

Table. 1 Natural frequencies, as determined by the preliminary FE model and measurement responses for the Gageocho ORS

Mode	1	2	3	4	5	RMSE
Measurement [Hz]	1.790	1.827	2.652	5.599	5.694	-
Preliminary model [Hz]	2.172	2.175	3.102	6.461	6.635	-
Error [%]	21.34	19.05	16.97	15.40	16.53	17.98

2.2 Root Cause Analysis for the Errors in Design and Construction

The causes for the above-mentioned errors were investigated to make the simulation model compatible with the measured result. The errors may simply be attributed to the inaccuracy of the simulation model, or the uncertainties of the construction process. Regarding the simulation model, the concrete and steel piles that were inserted into lower parts of jacket legs, as indicated in Figure 2(b), were omitted in the preliminary FE model. Additionally, the sections of the jacket legs in the splash zone were modeled as the most corroded. The reason for this was to ensure that the stiffness values of the main components in the jacket structure were underestimated so as to maximize the stress results for static analysis and ensure a more conservative safety estimation. However, these conditions resulted in highly discrepant dynamic characteristics, because the stiffness was underestimated and the considerable mass of the concrete was not considered.

In addition, only major members of the jacket structure, e.g., jacket legs, braces, and decks, were included in the preliminary model; therefore, the masses of various other components were applied as dead loads. The reason for this may have been to simplify the model for more efficient analysis. However, the total amount of the omitted

mass equates to more than 30% of the total mass of the modeled steel structures. Therefore, the dynamic properties, particularly the natural frequencies, which are fundamentally based on the ratio of stiffness to mass, were heavily exaggerated. Moreover, the center of mass cannot be precisely embodied, so the asymmetry between the strong axis and weak axis of the measured natural frequencies shown in Table 1 cannot be quantified.

Lastly, a significant contribution to construction error is the ambiguity of the strength of the concrete materials. To further explain, the specified compressive strength of concrete (f_{ck}) is assumed to be 28 GPa in the design stage (i.e., before construction), but, in practice, the 210 m³ cement is simply poured into the four jacket legs that are flooded with saline sea water (Woo et al. 2012). Considering the fact that the material properties of concrete are entirely dependent on the curing process, particularly the water-cement ratio, composition of the cement, temperature, and humidity, utilizing such a method to pour concrete increases the level of uncertainty of its material properties. This uncertainty may be one of the causes of the errors.

Table. 2 Causes of the discrepancy between the preliminary analysis results and Gagecho ORS measurements

	Reasons	Causes
Preliminary simulation model	Conservative safety check	Omission of concrete in jacket legs
		Omission of steel piles in jacket legs
		Modeling sections with the most corroded in splash zone
	Mass simplification	Regarding mass of equipment and other components as dead loads
Construction process	Uncertainty of material properties	Curing of concrete filled with seawater in flooded jacket legs

2.3 Direction of Model Updating

Among the possible causes that were previously mentioned, it would be relatively easy to correct the disregarded concrete and steel piles, and the corroded areas in the splash zone. However, it is difficult to exactly predict the material properties, such as the mass and stiffness of the concrete, due to uncertainty. Assuming that the legs are not broken, and thus there is no cement leakage, the total mass of the concrete filling in the legs can be considered as constant. Regardless of this assumption, the stiffness of the concrete remains to be unknown.

In addition to the concrete-related error, the equipment and other components that are simply regarded as dead loads in the preliminary FE model should be considered as individual masses. This is because, as mentioned earlier, the natural frequency theoretically reflects the ratio of stiffness to mass. More specifically, mass is one of the two fundamental contributions to natural frequency; therefore, a more accurate model of the mass elements would increase the accuracy of the updated simulation model. Moreover, in this case, it is also an important prerequisite for identifying the uncertain stiffness of the concrete. Because the stiffness is expected to have high uncertainty, the mass has to be exactly modeled to correctly find another

factor that contributes to the natural frequency, i.e., the unknown stiffness of the concrete. Therefore, in this study, a variety of mass element models were created and compared to determine which is most suitable for the model updating.

Various types of masses categorized as appurtenance, equipment, and facilities are listed in Table 3. The total number of masses exceeded 1000, and these masses were originally modeled as dead loads at their respective locations in the preliminary FE model. Therefore, every mass can be modeled at their initial locations. For example, a large number of different mass elements can be applied in the same location. However, they have a very complex distribution. Hence, it is quite inefficient, in the modeling and simulation processes, to individually model all of the masses at their own positions. For this reason, one equivalent mass was modeled for most of the masses, with the exception of the anodes, which were considered to have an integrated mass center; then, the one equivalent mass was reallocated in various ways. The reason for the exception is that, initially, the braces, i.e., a major structural member, are slender, and the anodes are attached to their centers. This means that the dynamic response of the braces is likely to be predominantly affected by the mass of the anodes. Additionally, the anodes are submerged, so their added mass has to be considered. Therefore, the dynamic characteristics of the braces will be inaccurately predicted if the locations of the anodes are ignored. It is for this reason that the anodes were individually modeled, unlike the other components.

Table. 3 Disregarded mass elements in the preliminary FE model, and their locations

Category	Item	Locations	Approach
Appurtenance	Anode	Brace	Individual Modeling
	Grating	Topside Decks	
	Handrail		
	Stair		
Equipment	Photovoltaic Power Generator		Topside Decks
	Hoist Crane		
	Rainwater Service Tank		
	Lantern		
	Wind Power Generator		
	Diesel Generator		
Facilities	Diesel Tank	Topside Decks	Integration & Reallocation
	Buildings		
	Walls		

2.4 Problem Definition and Pattern Search Method

In this research, updating the preliminary FE model was purposed to establish a model that is able to minimize the discrepancy between the calculated natural frequencies and the identified ones based on measurement, which are presented in Table 1. Therefore, the problem can be defined as an error minimization problem, as described by Eq. (1).

$$\min g = \sqrt{\sum_{i=1}^5 \left\{ W^i \times \left(\frac{f^i - f_m^i}{f_m^i} \right)^2 \right\}}, \quad (1)$$

where g is the objective function, i is the mode number, which ranges from 1 to 5, W^i , f^i , and f_m^i are the weight coefficient, the calculated natural frequencies, and the identified natural frequencies based on measurement for the i -th mode, respectively. The weight coefficients were applied as follows: 1 for the first bending modes (1st and 2nd natural frequencies), 0.5 for the first torsional mode (3rd natural frequency), and 0.25 for the second bending modes (4th and 5th natural frequencies). Basically, the natural frequency f^i is a function of the elastic moduli of the concrete and steel, as well as other parameters, depending on how the integrated mass is reallocated. Thus, it is reasonable that the respective moduli of elasticity of the concrete and steel are taken into account as updating parameters in the model updating.

However, the elastic modulus can theoretically range from 0 to infinity, so it is difficult to define the upper limit of its domain. Furthermore, as stated previously, it is difficult to accurately determine the value for concrete, meaning that a high computational cost would be required to find its global optimum. Therefore, the parameter θ , the tangent of which is equal to the normalized value of the elastic modulus, was introduced in this study (Eq. (2)).

$$\tan \theta = \frac{X - \mu_X}{\sigma_X} \left(\arctan \frac{-\sigma_X}{\mu_X} \leq \theta < \frac{\pi}{2} \right), \quad (2)$$

where X is an arbitrary unknown variable, and μ_X and σ_X are the mean value and standard deviation of the variable X , respectively. Regarding the mean, the elastic modulus values for the steel and concrete materials were assumed to be 200 GPa (E_s) and 27.7 GPa (E_c), respectively (Woo et al. 2012), in the design stage. For the standard deviation of the steel, a coefficient of variation (COV) of 0.06 was applied (Hess et al. 2002). However, the COV of the specified compressive strength of concrete (f_{ck}), which is the main factor affecting the tangential elastic modulus of concrete, has been reported to range between 0.04 and 0.2 (Baji 2014). Considering the imperfect and unclear concrete curing conditions, the largest value of 0.2 was used as the COV of concrete in this study.

Additionally, the pattern search (PS) method, which is one of global optimization techniques, was utilized to obtain the optimum solution of the updating problem described by Eq. (1). Specifically, the PS method directly searches for the optimum by iterating in steps, without utilizing the derivative information of an objective function, as follows: (1) a mesh comprised of points with the same pattern, e.g., the same equidistance from the current searching point, are set in variable space, (2) the values of the objective function for the points are calculated, and (3) the current point moves to the best (i.e., an optimal) point on the mesh if the objective function is less at the best point than at the current point; otherwise, a new mesh is generated with a shrinking pattern at the current point. Figure 3 (Jacquenot, 2009) displays an example of the convergence process of the PS method.

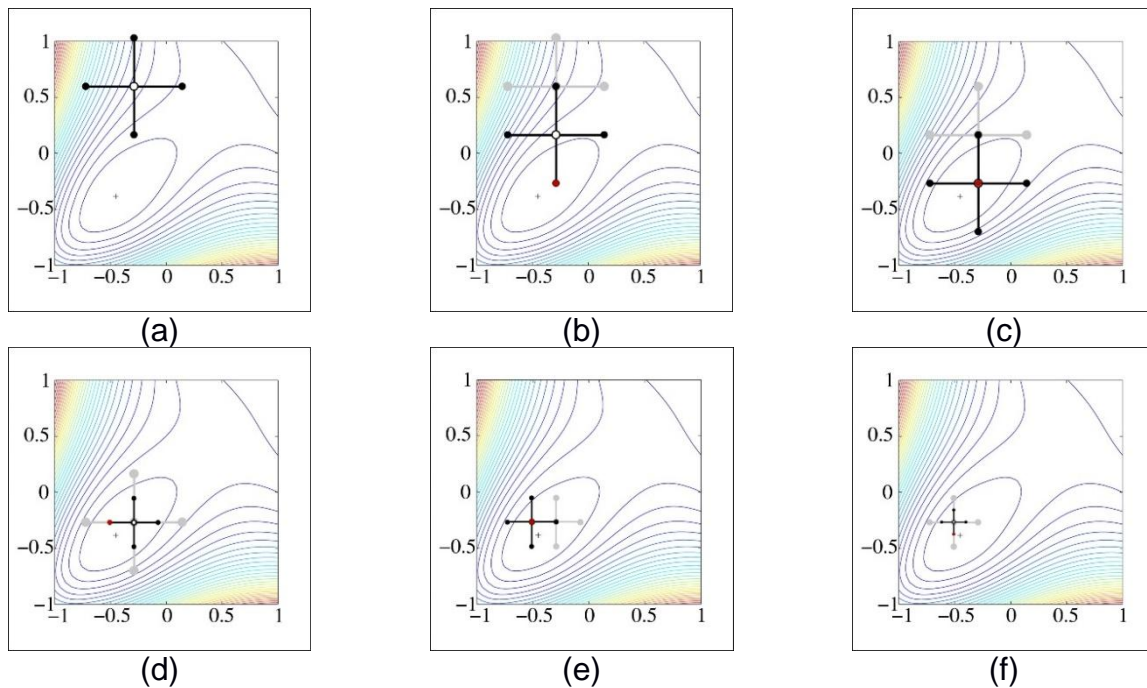


Fig. 3 Example of the convergence process of the PS method (Jacquetot 2009)

3. MASS MODELING CASES

3.1 Strategies for Mass Modeling and Additional Updating Parameters

The equivalent mass (M_T) of the ignored mass elements, and the location of the center (\vec{c}_T), are listed in Table 4. The total mass was approximately 90.49 ton, and it was eccentrically placed on the X-Y plane. The height of the center of mass was approximately 24.28 m, corresponding to the distance between the cellar deck and main deck (1st and 2nd floor decks, respectively), as shown in Figure 4. It should be noted that the heights of the three decks, i.e., the cellar, main, and roof decks, were as 22 m (Z_1), 26.5 m (Z_2), and 31 m (Z_3), respectively. The next step was determining how to embody the integrated mass in the FE model. This step is very important, as the natural frequencies calculated from the FE model are predominantly affected by how the integrated mass is applied. Furthermore, with the exception of the elastic moduli, updating variables are decided by the strategy of modelling the equivalent mass; therefore, the effectiveness of the model updating is also contingent on it. For these reasons, various strategies were applied, as described in Table 5 and Figure 5.

Table. 4 Equivalent mass and its location

Mass	Center of mass (\vec{c}_T)		
M_T [ton]	X_T [m]	Y_T [m]	Z_T [m]
90.491	0.040	0.765	24.278

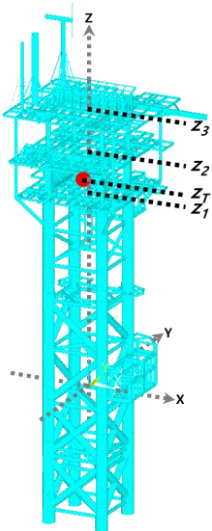
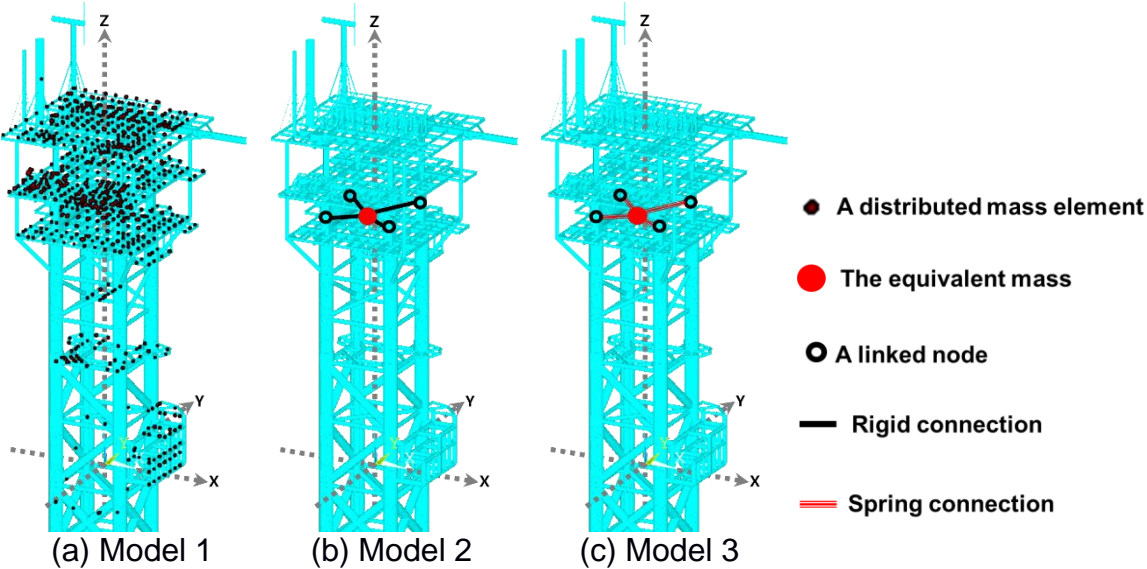


Fig. 4 Locations of the equivalent mass on the Gagecho ORS



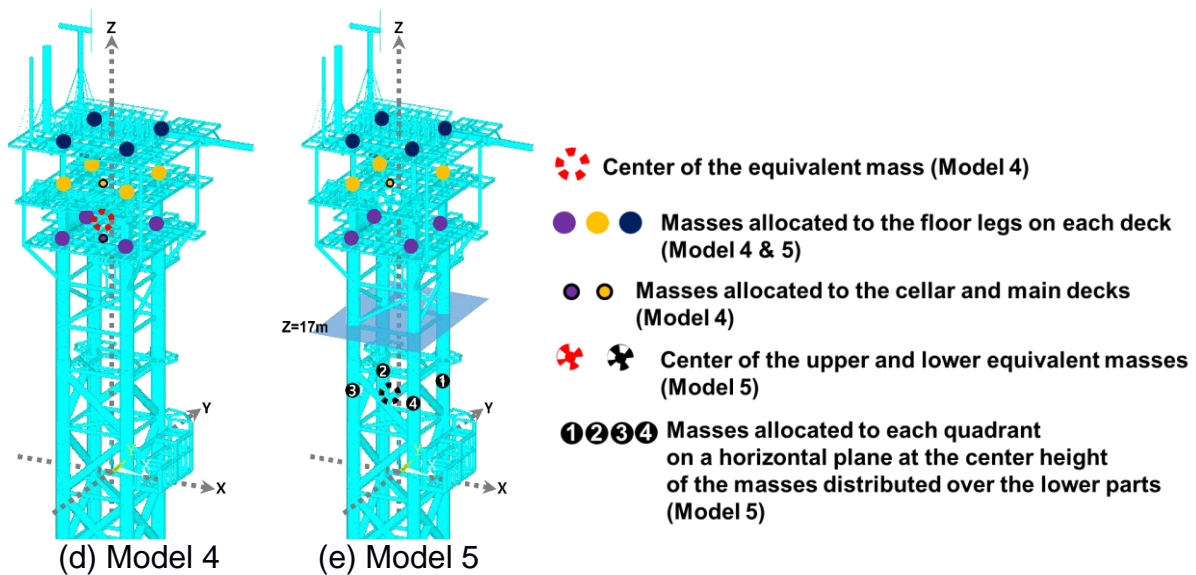


Fig. 5 Initial models based on the five strategies for the disregarded masses

Table. 5 Strategies to model the equivalent mass

	Approach	Updating Variables
1	Distributed mass elements	E_s, E_c
2	Equivalent mass with 4 rigid connections	E_s, E_c
3	Equivalent mass with 4 spring connections	$E_s, E_c, S_1, S_2, S_3, S_4$
4	Reallocation of masses on upper legs and deck nodes	E_s, E_c, α, β
5	Reallocation of masses on lower legs, upper legs and deck node	$E_s, E_c, \alpha, \beta, \gamma$

3.2 Model 1: Distributed Mass Elements

As illustrated in Figure 5(a), all dead loads were modeled as nodal mass elements. In the design report by Woo et al. (2012), it is stated that some of the dead loads were modeled as a single load, whereas the others were modeled as distributed loads; therefore, the distributed loads were transformed into several nodal mass elements. Consequently, 1,569 dead loads were modeled as a total of 3,083 nodal mass elements in this study. This task is generally highly complex and very time-consuming, so it was essential that it be very carefully performed. Considering the fact that the Gageocho ORS is a relatively small-scale and lightweight offshore structure, as compared to typical commercial offshore jackets in the oil and gas industries, it may be extremely difficult to apply this method to jacket structures that are much larger and more complex than the Gageocho ORS.

3.3 Model 2: Equivalent Mass with Four Rigid Connections

As shown in Figure 5(b), the integrated mass was rigidly linked to the closest node on each jacket leg. This can be considered as the most intuitive method, but the excessive stiffness resulting from the rigid connections may distort its dynamic characteristics.

3.4 Model 3: Equivalent Mass with Four Spring Connections

As described in Figure 5(c), uniaxial spring elements were used instead of the rigid connections, so their stiffness values were considered to be updating parameters. Unlike the steel members, the tensioners and compensators link components with stiffness; however, the spring connection elements do not actually exist. This means that the mechanical properties of physically nonexistent components have to be determined. Thus, this approach is likely to be somewhat controversial. Regardless of whether the assumption is practically reasonable, these variables contribute to the overall stiffness, so they were parameterized like the elastic modulus E_s , as shown in Eq. (2).

3.5 Model 4: Reallocation of Masses on Upper Jacket Leg and Deck Nodes

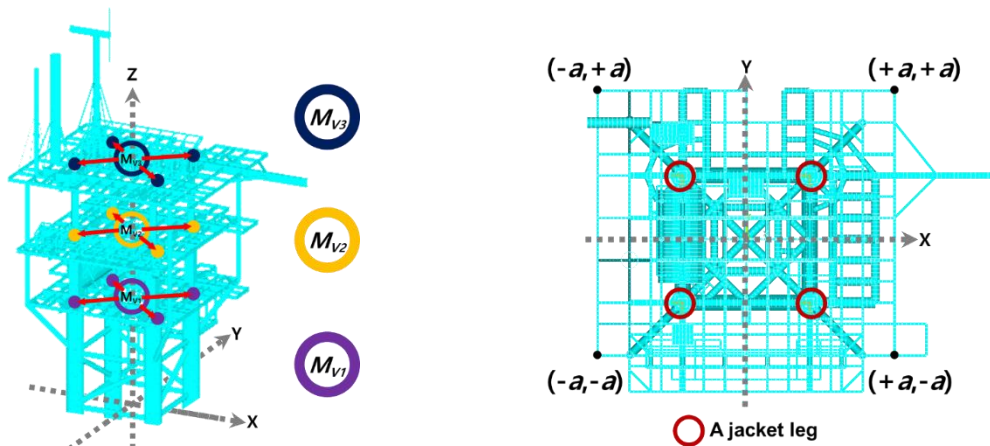
As seen in Figure 5(d), the integrated mass was reallocated to form two groups, with 12 nodes on the jacket legs, and two nodes on the decks. It should be noted that the nodal mass elements in the first group were redistributed across 12 nodes to represent the effects of mass distribution along the height of the structure, where the three deck planes intersect the four leg columns at right angles, because most mass elements were originally located on the three decks, as shown in Figure 5(a). Conversely, the elements in the second group were purposed to explicitly describe the eccentricity on the X-Y plane of the equivalent mass, so they were modeled on the deck planes.

The most important factor is the total mass (M_T); additionally, the center of mass (\vec{c}_T) had to be maintained before and after the reallocation, as described by Eqs. (3) and (4).

$$M_T = M_V + M_P, \quad (3)$$

$$M_T \cdot \vec{c}_T = M_V \cdot \vec{c}_V + M_P \cdot \vec{c}_P, \quad (4)$$

where M_V and M_P are the total masses applied to the 12 leg nodes and two deck nodes, respectively. \vec{c}_V and \vec{c}_P correspond to the centers of M_V and M_P , respectively. M_V was divided into M_{V1} on the 1st floor, M_{V2} on the 2nd floor, and M_{V3} on the 3rd floor, and the four intersection nodes on each deck shared equal portions of the mass, as shown in Figure 6(a). This means that the centers of M_{V1} , M_{V2} , and M_{V3} were always located at the origin of the X-Y plane, along with \vec{c}_V . Consequently, the only variable that was able to represent the horizontal effect of the center of mass was M_P , so the roles of the two mass-element groups were clearly distinguished. Regarding the vertical center of mass, it was assumed that M_V and M_P must be on the same level as M_T at Z_T .



(a) Mass allocation for the four jacket legs (b) Plan view of the Gageocho ORS

Fig. 6 Mass allocation for the legs, and a plan view of the Gageocho jacket structure

On the basis of the fundamental assumptions, the mass reallocation parameter α ($0 < \alpha < 1$) was introduced as the ratio of M_V to M_T , i.e., $M_V = \alpha M_T$ and $M_P = (1 - \alpha)M_T$. Then, Eq. (4) can be expressed as Eqs. (5) and (6). Eq. (6) shows that the center of M_P is only dependent on the parameter α .

$$M_T \cdot \vec{c}_T = \alpha M_T \cdot \vec{c}_V + (1 - \alpha)M_T \cdot \vec{c}_P = \alpha M_T \cdot (0, 0, Z_T)^T + (1 - \alpha)M_T \cdot (X_P, Y_P, Z_T)^T \quad (5)$$

$$\therefore (X_P, Y_P)^T = \frac{1}{1 - \alpha} (X_T, Y_T)^T \quad (6)$$

where X_P and Y_P are the horizontal coordinate values for the center of M_P . Additionally, it makes sense that M_P was placed within the range of the decks because, in actuality, all masses are within this range, as shown in Figure 5(a). Thus, as shown in Figure 6(b), X_P and Y_P were designed to be subject to the constraints presented in Eq. (7). Lastly, the parameter α for this model had the domain range defined in Eq. (8).

$$\begin{aligned} |X_P| \leq a, |Y_P| \leq a, \\ \frac{1}{1 - \alpha} |X_T| \leq a, \frac{1}{1 - \alpha} |Y_T| \leq a, \\ \alpha \leq 1 - \frac{|X_T|}{a}, \alpha \leq 1 - \frac{|Y_T|}{a}, \end{aligned} \quad (7)$$

$$\therefore 0 < \alpha \leq 1 - \frac{\max(|X_T|, |Y_T|)}{a}, \quad (8)$$

3.5.1 Reallocation of M_P

M_P was separated into M_{P1} and M_{P2} on the cellar and main decks, respectively. If M_P is applied to every three decks, the effect of mass momentum of equivalent mass on the dynamic characteristics can be represented by only M_P without M_V . In this case,

M_V would become meaningless, and M_P would be excessively large, thereby perturbing the dynamic modes and resulting in inaccurate model updates. More specifically, the local modes of the heavy masses applied to the slender and weak deck members could occur prior to the global modes of the structure, but this is not a realistic result. This is the reason why M_P was reallocated on the two decks (1st and 2nd floors) closer to the center of the equivalent mass.

The process of dividing M_P into M_{P1} and M_{P2} , and the equivalent mass momentum equilibrium, can be expressed as shown in Eqs. (9) and (10). These variables were transformed into a matrix, as shown in Eq. (11) to calculate the values for M_{P1} and M_{P2} (Eq. (12)).

$$M_P = M_{P1} + M_{P2}, \quad (9)$$

$$M_P \cdot Z_T = M_{P1} \cdot Z_1 + M_{P2} \cdot Z_2, \quad (10)$$

$$\begin{bmatrix} 1 & 1 \\ Z_1 & Z_2 \end{bmatrix} \begin{bmatrix} M_{P1} \\ M_{P2} \end{bmatrix} = (1 - \alpha) M_T \begin{bmatrix} 1 \\ Z_T \end{bmatrix}, \quad (11)$$

$$\therefore \begin{bmatrix} M_{P1} \\ M_{P2} \end{bmatrix} = (1 - \alpha) \frac{M_T}{Z_2 - Z_1} \begin{bmatrix} Z_2 - Z_T \\ Z_T - Z_1 \end{bmatrix}, \quad (12)$$

3.5.2 Reallocation of M_V

As was previously described for M_P , the equivalent mass and its center were applied to distribute M_V , as described by Eqs. (13) and (14).

$$M_V = M_{V1} + M_{V2} + M_{V3}, \quad (13)$$

$$M_V \cdot Z_T = M_{V1} \cdot Z_1 + M_{V2} \cdot Z_2 + M_{V3} \cdot Z_3, \quad (14)$$

Similar to the method for defining the parameter α , the ratio of M_{V1} to M_V is defined as the parameter β ($0 < \beta < 1$), as shown in Eq. (15). Subsequently, Eqs. (13) and (14) can be obtained as the function of M_{V2} and M_{V3} by substituting M_{V1} with $\beta \cdot M_V$ in Eq. (15) to yield the matrix shown in Eq. (16).

$$M_{V1} = \beta M_V, \quad (15)$$

$$\begin{bmatrix} 1 & 1 \\ Z_2 & Z_3 \end{bmatrix} \begin{bmatrix} M_{V2} \\ M_{V3} \end{bmatrix} = M_V \begin{bmatrix} 1 - \beta \\ Z_T - \beta Z_1 \end{bmatrix}, \quad (16)$$

$$\therefore \begin{bmatrix} M_{V2} \\ M_{V3} \end{bmatrix} = \frac{M_V}{Z_3 - Z_2} \begin{bmatrix} Z_3 - Z_T - \beta(Z_3 - Z_1) \\ Z_T - Z_2 + \beta(Z_2 - Z_1) \end{bmatrix}, \quad (17)$$

It is certain that M_{V2} and M_{V3} cannot be negative, so the range of β can be obtained as shown in Eq. (18); then, M_{V1} , M_{V2} , and M_{V3} can be formulated by replacing M_V with $\alpha \cdot M_T$ and utilizing α , β , and M_T as shown in Eqs. (19) and (20).

$$\frac{Z_2 - Z_T}{Z_2 - Z_1} \leq \beta \leq \frac{Z_3 - Z_T}{Z_3 - Z_1}, \quad (18)$$

$$M_{V1} = \alpha\beta M_T, \quad (19)$$

$$\left| \frac{M_{V2}}{M_{V3}} \right| = \frac{\alpha M_T}{Z_3 - Z_2} \left| \frac{Z_3 - Z_T - \beta(Z_3 - Z_1)}{Z_T - Z_2 + \beta(Z_2 - Z_1)} \right|, \quad (20)$$

As a result of this formulation method, the natural frequency of the i -th mode, f^i , in the objective function of Model 4 is a function of the mass reallocation parameters α and β , as well as the elastic moduli of the steel and concrete. Therefore, the four parameters are updating parameters.

3.6 Reallocation of masses on Four Lower and Upper Jacket Legs and Deck Nodes

Despite the fact that the reallocation of the integrated mass to the platform seems reasonable by virtue of the fact that the centers of the equivalent masses are placed at the levels of the decks, considering the effects of the moment of inertia on the natural frequencies, there may be a limit to how precisely the model can reflect the conditions of the actual structure, because the masses are actually distributed throughout the entire structure, even far from the center, as shown in Figure 5(a). For this reason, two different mass groupings that were centered at 17 m above sea level were set as M_U and M_L , corresponding to the upper and lower parts, respectively, before being independently reallocated as illustrated in Figure 5(e).

Table 6 provides the values of M_U and M_L , in addition to the corresponding coordinates of the centers of mass, \vec{c}_U and \vec{c}_L . Specifically, Z_U was 26.1841 m, so M_U was very close to the main deck, because the masses included in the lower part were excluded. The distance to the floor was only approximately 0.3 m, which does not seem very significant considering the fact that the spacing between the decks is 4.5 m. Thus, M_{UP} , corresponding to M_p of Model 4, was not shared between two decks, but only applied to the middle deck. Conversely, M_{UV} was determined exactly as described for M_V in Model 4. Therefore, the mass reallocation parameters α and β shall be included in updating parameters, as the Model 4. One difference is that the approximation of M_{UP} causes the parameter β to be dependent on the parameter α ; therefore, the search area for β was updated based on the results of α at each iteration.

Table. 6 Equivalent masses and their locations (Model 5)

	Mass [ton]	Center of mass (\vec{c}_U & \vec{c}_L)		
		X [m]	Y [m]	Z [m]
M_U [ton]	80.592	-0.0697	0.5099	26.1841
M_L [ton]	9.899	0.9313	2.8451	8.7615

3.6.1 Reallocation of M_L

As listed in Table 6, M_L was 9.899 ton, meaning that approximately 10% of the integrated masses were distributed below 17 m. X_L and Y_L were 0.93 m and 2.85 m, respectively, so the center of M_L was much more eccentric than that of M_T . This is

because X_L and Y_L were farther from the origin on the X-Y plane than X_T and Y_T . Therefore, how to accurately model the eccentricity was the main consideration for M_L . It should also be noted that there was no planar member in the lower parts, so M_L had to be shared among the four nodes on the legs.

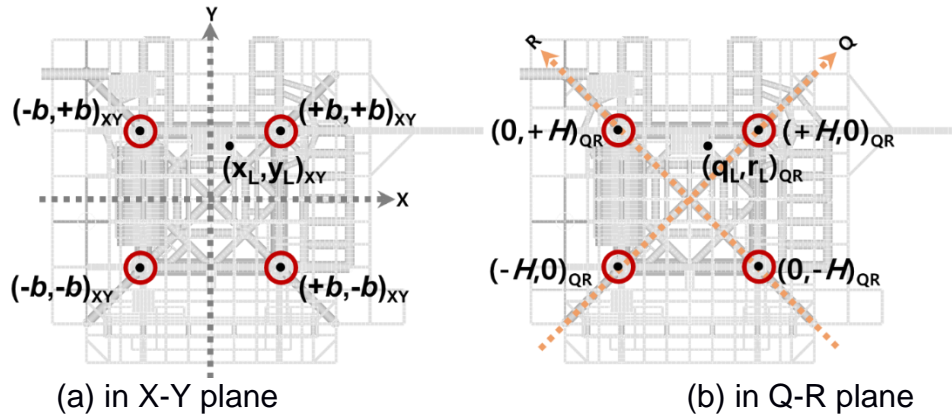


Fig. 7 Plan views of the Gagecho jacket structure

For a more intuitive derivation of M_L , the Q-R plane coordinates were utilized instead of the global X-Y planar coordinates. The Q and R axes corresponded to a 45° rotation of the X and Y axes, respectively, about the positive Z axis, as shown in Figure 7. As previously described, the conservation of M_L , and its center, before and after this reallocation was applied as described via Eqs. (21), (22), and (23), and the reallocated nodal mass at any leg point on one of the four legs (e.g., M_Q^- at $(-H, 0)_{QR}$), can be expressed by creating a new reallocation parameter γ ($0 < \gamma < 1$), as shown in Eq. (24). These four equations can be written in matrix form (Eq. (25)); then, the amounts of the four nodal masses can be calculated by solving Eq. (26).

$$M_L = M_Q^+ + M_Q^- + M_R^+ + M_R^- \quad (21)$$

$$M_L \cdot q_L = M_Q^+ \cdot H + M_Q^- \cdot (-H) \quad (22)$$

$$M_L \cdot r_L = M_R^+ \cdot H + M_R^- \cdot (-H) \quad (23)$$

$$\gamma \cdot M_L = M_Q^- \quad (24)$$

$$\begin{bmatrix} 1 & 1 & 1 & 1 \\ H & -H & 0 & 0 \\ 0 & 0 & H & -H \\ 0 & 1 & 0 & 0 \end{bmatrix} \quad (25)$$

$$\therefore \begin{bmatrix} M_Q^+ \\ M_Q^- \\ M_R^+ \\ M_R^- \end{bmatrix} = M_L \begin{bmatrix} 0 & \frac{1}{H} & 0 & 1 \\ 0 & 0 & 0 & 1 \\ \frac{1}{2} & -\frac{1}{2H} & \frac{1}{2H} & -1 \\ \frac{1}{2} & -\frac{1}{2H} & -\frac{1}{2H} & -1 \end{bmatrix} \begin{bmatrix} 1 \\ q_L \\ r_L \\ \gamma \end{bmatrix} \quad (26)$$

Additionally, all elements comprising the vector on the right-hand side of Eq. (26) are positive. Note that, although M_Q^+ and M_Q^- are always mathematically positive under such conditions, the others can sometimes be negative. However, the mass has to be non-negative, and M_R^- is always less than M_R^+ . Therefore, an appropriate condition for the non-negative nodal masses in this problem is a non-negative M_R^- . This can be expressed as shown in Eq. (27). Additionally, the feasible range of the parameter γ was determined to be as shown in Eq. (28).

$$M_R^- = M_L \left(\frac{1}{2} - \frac{q_L}{2H} - \frac{r_L}{2H} - \gamma \right) \geq 0 \quad (27)$$

$$\therefore 0 < \gamma \leq \frac{1}{2} \left(1 - \frac{q_L + r_L}{H} \right), \quad (28)$$

Consequently, the five parameters, i.e., the respective moduli of elasticity E_s and E_c of the steel and concrete, and three mass reallocation parameters (α , β , and γ), were taken as the updating parameters in this model.

4. UPDATING RESULTS AND DISCUSSION

4.1 Results Summary

Table 7 lists the lowest five natural frequencies, root mean square errors (RMSEs), and the objective function values of eight different models. Table 8 presents the values of the two types of elastic moduli that were applied in all models and the updated results of the two elastic moduli for steel and concrete obtained from different initial models.

4.2 Modified Model

In general, the proposed model is the preliminary FE model that has been revised to consider the corroded areas, and the concrete and steel piles in the four jacket legs. Regarding the natural frequencies obtained via the preliminary FE model, although the errors of the preliminary model (relative to the measured results) were larger than approximately 15% for all modes, the errors of the modified model were less than approximately 15% for every mode. The RMSE values also decreased from approximately 17.98% to 14.52%. In particular, the errors for lower modes, which were considerably larger than those for the higher modes in the preliminary FE model, decreased by nearly 6%.

Table. 7 Comparative Result Summaries

Mode	Natural frequencies [Hz]					RMSE [%]	Objective function
	1	2	3	4	5		
Measurement	1.790	1.827	2.652	5.599	5.694	-	-
Modified model	2.061	2.065	2.999	6.472	6.579	14.524	-
(Error [%])	15.14	13.03	13.08	15.59	15.54		
Model 1_Initial	1.843	1.845	2.283	4.109	5.146	14.175	0.17518
(Error [%])	2.961	1.007	-13.910	-26.621	-9.628		
Model 1	1.827	1.829	2.385	4.133	5.308	12.943	0.08680
(Error [%])	2.041	0.120	-10.08	-26.19	-6.772		
Model 2_Initial	2.119	2.124	5.919	6.013	6.368	56.516	0.90761
(Error [%])	18.380	16.267	123.179	7.398	11.832		
Model 2	1.634	1.639	4.070	4.955	5.329	25.358	0.30127
(Error [%])	-8.734	-10.27	53.48	-11.50	-6.416		
Model 3	1.596	1.984	2.736	5.263	5.306	7.530	0.14091
(Error [%])	-10.815	8.596	3.184	-6.002	-6.820		
Model 4_Initial	1.904	1.906	2.649	5.658	5.739	3.491	0.07721
(Error [%])	6.346	4.346	-0.128	1.056	0.790		
Model 4	1.807	1.810	2.653	5.617	5.644	0.736	0.01372
(Error [%])	0.962	-0.950	0.032	0.324	-0.880		
Model 5	1.807	1.809	2.654	5.586	5.685	0.631	0.01384
(Error [%])	0.973	-0.981	0.066	-0.232	-0.167		

Table. 8 Elastic moduli E_c and E_s , corresponding to the updated results for each model in Table. 7

Model	Modified model	Optimum value				
	Model 1&2_Initial	Model 1	Model 2	Model 3	Model 4	Model 5
E_c [GPa]	27.7	0.000	17202055	0.000	8.010	6.084
E_s [GPa]	200	234.612	70.052	171.310	201.107	215.407

4.3 Distributed Masses: Model 1

The modified FE model was revised by considering all nodal masses. Initially, the two types of elastic moduli in the preliminary model were identical to those in the modified model, as given in Table 8; the results are listed in Table 7 as Model 1_Initial. For the modified model, the first two natural frequencies were significantly lower and relatively similar to the measured values. This can be considered to be a result of modeling the originally disregarded masses in the modified FE model. However, the RMSE only decreased by approximately 0.4% because the error of the 4th natural frequency increased.

The optimal values of the elastic moduli of the concrete and steel material were updated based on the Model 1_Initial value; the optimal E_c and E_s values, and their corresponding resultant natural frequencies, are summarized in Tables 7 and 8 (Model 1). It can be ascertained that the errors in Table 7 decreased by approximately 1~3% relative to the Model 1_Initial results. Although this can be attributed to the effect of optimization, the updated FE model does not seem to accurately represent the actual structure for several reasons. The first reason is that the errors for the 3rd to 5th modes were relatively large, and, particularly, the 4th natural frequency error reached 25%. Secondly, the RMSE of approximately 12.94% for Model 1 is not sufficient to ensure agreement with the measured data. Lastly, not only was the optimized E_c less than 1 MPa, which is too small, even considering its uncertainty, but the optimized E_s was also significantly larger than expected, i.e. the updated value of E_s exceeded 2.83 standard deviation of the mean (i.e. the design target value of the steel).

4.4 Equivalent Nodal Mass: Model 2 and Model 3

Regarding Models 2 and 3, the overall results, including those for the natural frequency errors, RMSEs, and optimum values of E_c and E_s , prove that these models are inadequate. This is especially evidenced by the optimal moduli of elasticity results. Specifically, the values for both types of materials were impossibly large. The reason for this is that the equivalent mass was modeled as one nodal mass at the center of mass.

Regarding Model 2, the initial model and design values for the elastic moduli are presented as Model 2_Initial, and its natural frequencies are listed in Table 7. As compared to Model 1_Initial, every natural frequency increased by at least 15%; particularly, the 3rd natural frequency increased by nearly 160%. This means that the stiffness significantly increased, mainly affecting the torsional as well as bending behavior of the structure. The primary cause of this was the rigid connections to the equivalent mass. The connections rigidly linked four jacket legs to one another through the mass near the free end, and their effects overwhelmed the effect of the equivalent mass. Thus, the main problem became how to compensate for the influence of the rigid connections, but not the equivalent mass.

In this regard, the optimization process converged in the direction in which the effective length of the dynamic response of the structure decreased as a result of the elasticity of the concrete substantially increasing, as can be seen in Table 8. This resulted in all concrete components becoming too stiff to move; therefore, the height of the only movable parts above the concrete column became the effective dynamic length. The mode shapes for Model 2, as described in Figure 8, also supports this hypothesis. As the concrete components stiffened, the steel materials became very compliant to compensate for the increasing stiffness brought about by the rigid connections and rigid concrete. This is because the objective function, i.e., the weighted RMSE, drove the convergence process to mainly controlling the bending stiffness, which consequently reduced the errors of four modes, i.e., excluding the 3rd torsional mode. Although the effects of such a convergence process caused all of the natural frequencies to decrease by at least 15% relative to the Model 2_Initial results, its RMSE was still larger than that for Model 1, Model 1_Initial, and the modified model. The reason for this is that the effects of the rigid connections on the torsional mode

were more significant on other bending modes, and that the bending and torsional stiffness were differently affected by those parameters.

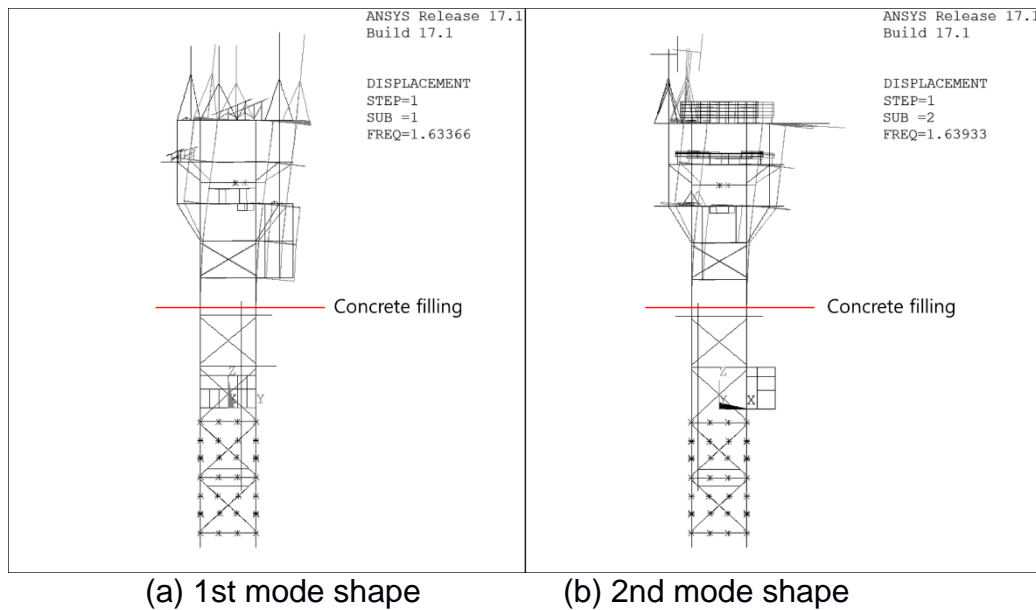


Fig. 8 Mode shapes for Model 2, overlapped with their corresponding non-deformed shapes (auto-scaled)

Model 3 was a trial to overcome such the shortcomings of Model 2, so 4 axial springs were applied instead of the rigid connection. In this case, however, local motions of the equivalent nodal mass are fairly likely to occur prior to the global behavior of the entire structure. In fact, the nodal mass rather separately vibrates with its own mass and stiffness as illustrated in Figure 9, like seismic dampers for earthquake-proof, such as a tuned mass damper (TMD), although the motion is not perfectly independent with the behavior of the whole structure. For this reason, 3rd to 7th eigen frequencies of Model 3 corresponding to 1st to 5th natural frequencies of the jacket were used.

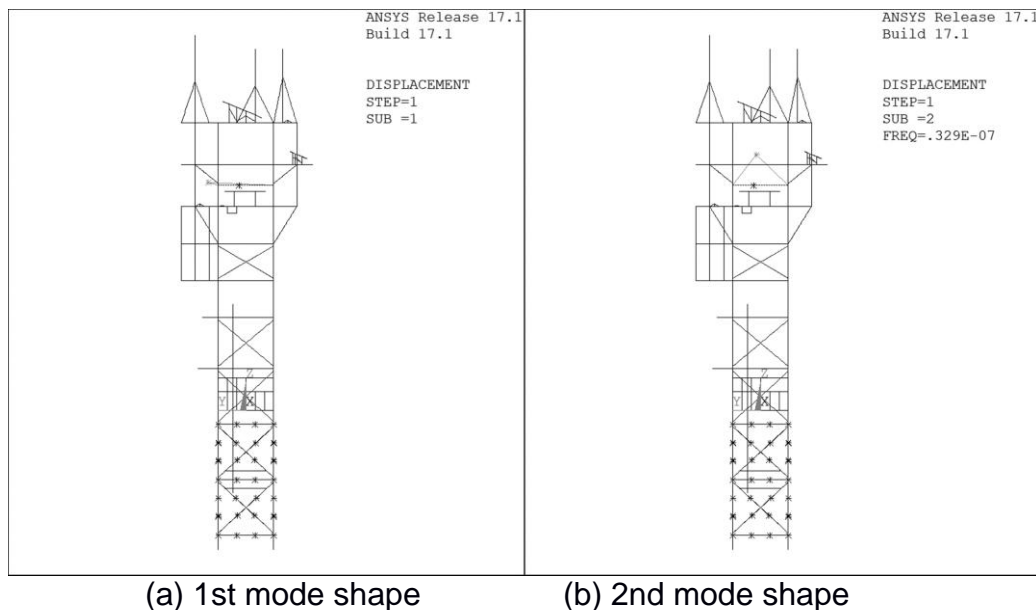


Fig. 9 Mode shapes of Model 3, overlapped with undeformed shape (auto scaled)

In the actual structure, the horizontal eccentricity seen in the measured natural frequencies would be attributed to distribution of masses under the assumption that there is no damage on the jacket. On Model 3, however, the stiffness of the virtual connections (S_1 to S_4 on Table 5) would have mainly influence on the eccentric behavior of Model 3, not only the equivalent nodal mass. For instance, even if the natural frequencies be well matched with each other, mode shapes, more specifically, the strong and weak axes may be different with the real Gagecho ORS; fortunately, such the issue did not happen in the optimal Model 3, though. Therefore, something different manner capable of evaluating the agreement of mode shapes, such as modal assurance criterion (MAC), would be required for this case.

4.5 Mass Reallocation Method: Models 4 and 5

As shown in Table 7, all of the errors for the 1st to 5th modes were significantly reduced, and in the cases of Models 4 and 5, the errors were reduced to less than 1%. In particular, the errors corresponding to the 3rd natural frequency substantially decreased to less than 0.1%. It is noteworthy that that the accuracy of the 3rd mode, i.e., a torsional mode, may be an important factor that affects the ability of the model to precisely update the preliminary model. The rationale behind this is that there are no slight differences, depending on the X- and Y-axes, between the 1st and 2nd and 4th and 5th measured natural frequencies, and that they would be predominantly attributable to the eccentricity of the masses. This would limit the amount that the overall error could be reduced for all modes, including the two 1st-bending and two 2nd-bending natural frequencies, if the effect of the eccentric mass on the horizontal plane is not properly represented. Therefore, the 1st torsional mode can be considered as a direct parameter to evaluate the accuracy of the model updating in this case.

The optimized elastic modulus values are considered to be more suitable than the previously determined optimized values. The intuitive criterion for this is the optimization of the elastic modulus of the steel. This is because the properties of steel

are generally easier to determine than those of concrete due to its uncertainty in curing process. It is known that the modulus of elasticity of steel is typically within the range of approximately 200–215 GPa, and the COV is considered as less than 0.06 (Hess et al. 2002). Considering this, the two optimized values of 201.11 GPa and 215.41 GPa (Table 8) for Models 4 and 5, respectively, are practical within one standard deviation from the initial value (i.e. design value). Therefore, these values verify the accuracy of Models 4 and 5, indicating that the steel structure would not incur any serious damage. Consequently, all of the concrete would remain in the jacket legs and not leak out into the sea. However, the optimized moduli of elasticity for Models 4 and 5 were less than one-third of the design value. Therefore, under the assumption that leakage did not affect the mass or density, the most reasonable reason for the lower moduli of elasticity is improper concrete curing.

Regarding the reallocated masses, Table 9 shows the results for M_V , M_P , and M_L (M_Q^+ , M_Q^- , M_R^+ , M_R^-). The masses of 66.74 and 23.76 ton were reallocated to M_V and M_P , respectively, in the case of Model 4. This means that approximately 26.25% of the equivalent mass contributes to the horizontal eccentricity of the dynamic response. This is considered to be an advantage, as it is possible to precisely determine the amount of mass that contributes to the eccentric dynamic properties. However, it is not easy to intuitively interpret the eccentric portion of the equivalent mass in Model 5 because of M_L . Hence, the difference between the opposing masses, $|M_Q^+ - M_Q^-|$ and $|M_R^+ - M_R^-|$, were regarded as the effective eccentric mass in this study, in consideration of the relationships between the center of mass and the masses and moment arms. Based on this, the eccentric portion of the equivalent mass in Model 5 was determined to be approximately 21.785 ton, which is slightly less than that in Model 4. The reason for this is that the eccentric mass can be distributed along height of a structure, so Model 5 is able to model this more precisely than Model 4. This is a merit of Model 5.

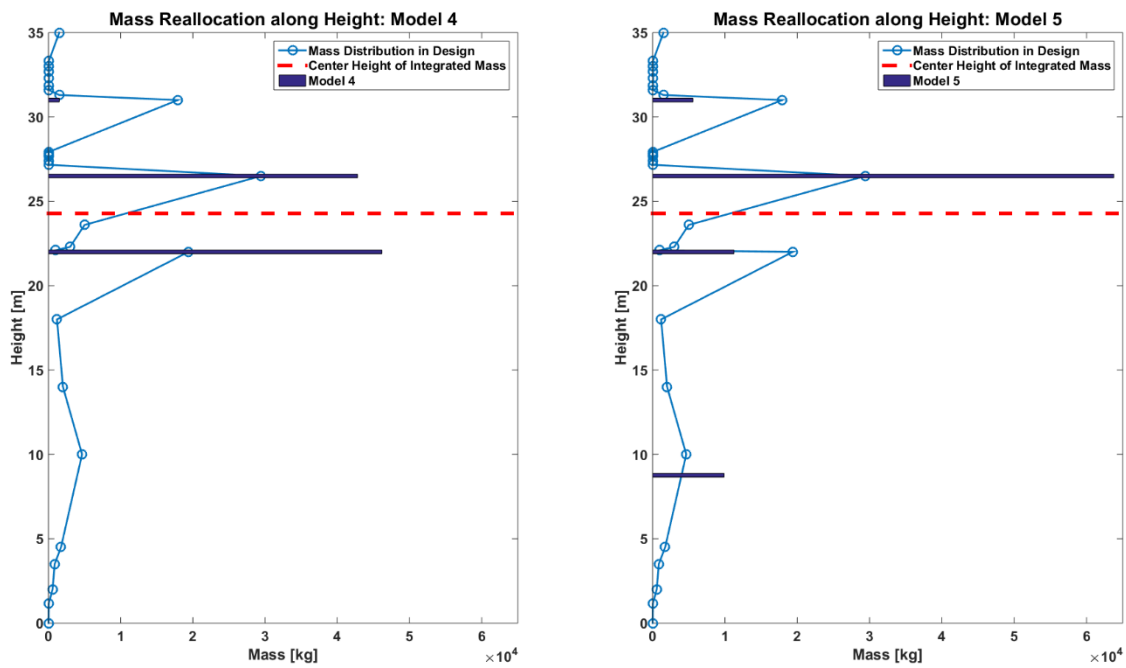
Table. 9 Reallocated masses of Models 4 and 5

	M_V	M_P	M_Q^+	M_Q^-	M_R^+	M_R^-
Model 4 [ton]	66.735	23.756	-	-	-	-
Model 5 [ton]	61.880	18.712	6.231	3.413	0.000	0.256

Lastly, Table 10 presents the masses with respect to the vertical height, and it also provides a comparison, showing that the simulated masses overlapped with the original mass distribution. In Model 4, most of the equivalent mass was reallocated to on the main and cellar decks. This is because M_P was only shared between the two decks. This allocation method did not yield results that were well-matched with the original mass distribution. Conversely, most of the mass was concentrated on the main deck in the case of Model 5. The reason for this is that the upper masses were nearly symmetrically distributed about the main deck. Consequently, the tendency of mass reallocation in Model 5 was better representative of the actual mass ratio for the three decks.

Table. 10 Masses according to vertical height

	Model 4	Model 5
Roof [ton]	1.505	5.591
Main [ton]	42.799	63.752
Cellar [ton]	46.187	11.249
Lower legs [ton]	0	9.899
Total [ton]	90.491	90.491



(a) Model 4

(b) Model 5

Fig. 10 Mass reallocation along height

5. CONCLUSIONS

In this study, FE model updating was carried out for the Gagecho ORS, which was retrofitted after incurring severe damage as a result of Typhoon Muifa in 2011, on the basis of its measured dynamic characteristics; the following conclusions were made:

- (1) It was found that the natural frequencies obtained via the design drawing-based preliminary FE model did not match well with those obtained via measurements; the primary causes were analyzed and classified as modeling and construction errors. In particular, the concrete fillings and extra masses that were disregarded in the model were considered to be the main sources of this large discrepancy; hence, these parameters were treated as the main parameters to be updated.
- (2) Five different initial FE models were established; then, which model is most suitable for model updating was investigated by evaluating their updated parameters, i.e., the elastic moduli of the steel and concrete components, and the

- RMSE of the natural frequencies that were derived from the updated FE models (relative to the corresponding measured natural frequencies).
- (3) Regarding the updated parameters of Model 1, an RMSE of nearly 29%, and elastic modulus of steel, even under the condition of very conservative calculations, revealed that modeling every mass in their respective locations is not accurate or effective.
 - (4) Based on the updated results of Models 2 and 3, it was found that modeling one equivalent nodal mass at the center of mass resulted in a connection problem, regardless of whether the links were rigid or spring. The rigid connections substantially increased the stiffness owing to the rigidly linked jacket legs in Model 2, whereas the spring connections increased the complexity of the optimization process in Model 3.
 - (5) The mass reallocation method did not result in any connection problems and was less time-expensive than modeling all of the nodal masses. The updated FE models that were based on the initial Models 4 and 5 yielded very small errors, i.e., less than 1% for all the five modes, and the updated values of elastic modulus of steel were also reasonable. This accuracy was credited to the ability of the models to effectively represent the effects of mass eccentricity, as well as the characteristics of the global dynamic response according to the height of masses.
 - (6) Employing the mass reallocation method enabled quantification of the amount of mass that contributed to the dynamic eccentricity, thereby demonstrating the importance of precise identification of the eccentricity in model updating based on structural dynamic properties.
 - (7) The calculated stiffness of the concrete grouting is expected to be significantly less than the design target capacity. One of the primary causes of this is speculated to be related to the underwater concrete curing conditions.

REFERENCES

- Anslys Inc. (2017), "Ansys Mechanical Advanced Parametric Design Language v17.1".
- Baji, H. (2014), "The effect of uncertainty in material properties and model error on the reliability of strength and ductility of reinforced concrete members", PhD dissertation, University of Queensland.
- Cremona, C. and Santos, J. (2018), "Structural Health Monitoring as a Big-Data Problem", *Structural Engineering International*, 28(3), 243-254.
- Engineering Dynamics, Inc. (1995), "SACS USER'S MANUAL Release 4".
- Fritzen, C.P., Klinkov, M., Kraemerbbs, P. and Koranyi, B. (2013), "Vibration-Based Damage Diagnosis and Monitoring of External Loads", W. Ostachowicz and J.A. Güemes (eds.), *New Trends in Structural Health Monitoring*, 24, 149-208.
- Jacquenot, G. (2009), "Example of convergence of a direct search method on Broyden function", https://commons.wikimedia.org/wiki/File:Direct_search_BROYDEN.gif. (Accessed 11 August 2019)
- Hess, P.E., Bruchman, D., Assakkaf, I.A. and Ayyub, B.M. (2002), "Uncertainties in Material and Geometric Strength and Load Variables", *Naval Engineers Journal*, 114(2), 139-166.

- Kim, W., Yi, J.H., Min, I.K. and Shim, J.S. (2017), "Estimation of Dynamic Characteristics of Gageocho Ocean Research Station using Long-term Measurement Data", *Journal of Coastal Disaster Prevention*, 4(5) [special issue], 263-270. (in Korean)
- Shim, J.S., Chun, I.S., Min, I.K. and Kim, S.S. (2015), "A study on damage recovery for Gageocho ocean research station", *KSCE 2015 Convention & Civil Expo*, 237-238. (in Korean)
- The MathWorks, Inc. (2015), "MATLAB and Global Optimization Toolbox Release 2015a", Natick, Massachusetts, United States.
- Woo, C. and Sin, J. (2012), "Precision Safety Diagnosis and Disaster Recovery Design of Gageocho Ocean Research Station", Report No. BSPE98689-10169-7, Korean Ocean Research & Development Institute. (in Korean)